

# Computation of hypersonic shock boundary layer interaction on a double wedge using a differential Reynolds Stress Model

A. Bosco

AICES, Templergraben 55, Aachen, 52056, Germany

B. Reinartz

CATS, Theaterplatz 14, Aachen, 52062, Germany

S. Müller

IGPM, Templergraben 55, Aachen, 52056, Germany

The simulation of hypersonic flows presents some difficulties due to the interaction between boundary layers and shock waves and to the high total enthalpy. In order to achieve more accurate numerical results with respect to physics, a Reynolds stress model (RSM) has been implemented in the well validated Reynolds averaged Navier-Stokes solver QUADFLOW. The RSM developed and tested by Einfeld, showed promising results on structured grids. It is a combination of two RSM: one that performs better near the wall and another able to achieve good results in the far field. The implementation consisted of writing new routines for the source terms and their derivatives as well as modifying routines for the computation of viscous fluxes, boundary conditions and far field conditions. The newly implemented model has been tested and validated on the standard test case of a subsonic flat plate and on a hypersonic configuration. The results show a good agreement between the experimental data and the solutions obtained with standard turbulence models implemented in the same software. A grid convergence study and a simulation on a complete three dimensional inlet are being performed.

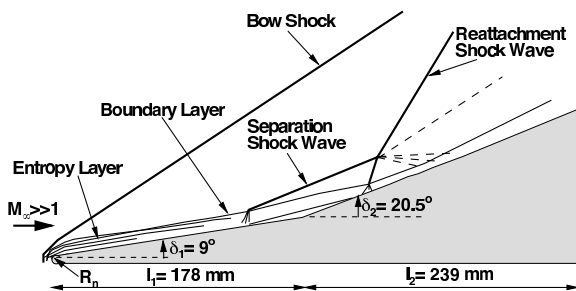


Figure 1. Shock / boundary layer interaction on a double wedge (Reinartz et al. (2007)).

## 1. Introduction

The aerodynamic design of hypersonic inlets is a critical issue for the overall performance of an air breathing propulsion system. Two phenomena characterize the technological problems of the inlet: on the one hand, the interaction of strong shock waves with thick hypersonic boundary layers causes large separation zones that reduce the captured mass flow and thus the engine performance. On the other hand, the high total enthalpy of the flow leads to severe aerodynamic heating, further enhanced by turbulent heat fluxes.

Currently, most of the turbulent flows are studied through the mean of the Reynolds Averaged Navier-Stokes (RANS) method, where the averaged governing equations are solved for the mean variables. One of the main issues of the RANS approach is to model the terms, mainly the Reynolds stress tensor, that appear after the averaging process and describe the turbulent contribution to the mean flow.

In order to model the Reynolds stresses, eddy viscosity models are widely employed since they are easy to implement and computationally convenient. Nevertheless these models show difficulties to correctly predict flow phenomena like shock boundary layer interaction, which are of great interest for hypersonic flow.

One of the limits of eddy viscosity models is that turbulence is modeled as an isotropic quantity. This hypothesis is not suitable for hypersonic flows where the strongly anisotropic flow phenomena, taking place in the boundary layer, have a great influence on the overall flow. For this reason a differential Reynolds stress model (Einfeld (2004), Einfeld et al. (2005)) -the SSG/LRR- $\omega$  model- has been implemented into QUADFLOW (Bramkamp et al. (2004)). This solver is a parallel adaptive compressible flow solver which employs locally refined meshes with hanging nodes. The model chosen in this article has been developed by Einfeld, who implemented it in the flow solver FLOWer for structured grids (Kroll et al. (2000)).

Until now the SSG/LRR- $\omega$  model has been implemented into QUADFLOW. It has been tested on a subsonic flat plate and on a hypersonic double wedge configuration (Figure 1). The results obtained have been compared with experimental data in Reinartz et al. (2007) and numerical results obtained from other turbulence models. In this paper a comparison with the SST Menter turbulence model for the hypersonic double wedge is presented. The choice of implementing a RSM in QUADFLOW is motivated by the promising results obtained by the same model with the FLOWer solver especially for separated flows.

## 2. QUADFLOW Solver

QUADFLOW solves the Euler and Navier-Stokes equations around complex aerodynamic configurations. It uses a cell-centered finite volume method on locally refined grids. The grid adaptation is based on a multiscale analysis and data compression similar to techniques used for im-

age compression. This is a new strategy independent of error indicators and error estimators. The fundamental idea is to rewrite an array of cell averages by which the flow field at hand is characterized into a new data format that allows for data compression. By means of the compressed data the grid adaptation is performed. The details of this strategy and its analysis as well as computational aspects can be found in Bramkamp et al. (2004). The computational grids are represented by block-structured parametric B-Spline patches.

For the computation of the convective flux, the flux-difference splitting HLLC Riemann solver by Batten and Leschziner (Batten et al. (1997)) is chosen. This method is capable of exactly preserving isolated shocks, contact and shear waves and it enforces the entropy condition in a way that no entropy correction of the primitive variables is employed.

For what concerns the computation of the viscous fluxes, the gradients of the variables at cell interfaces are determined using the divergence theorem. The computations presented here are steady state analyses so that time plays the role of an iteration parameter to achieve asymptotically stationary flow in the computation. The numerical methods employed are a Runge-Kutta fifth-order explicit scheme. In the QUADFLOW solver different turbulent models can be chosen. These are all RANS eddy viscosity models, in which the same proportionality between Reynolds stress tensor and the strain rate tensor as for the viscous stresses of a Newtonian fluid in laminar flow is considered. Even though these models are easy to implement and computationally convenient, they appear to be not suitable to simulate flow phenomena like shock boundary layer interaction in hypersonic flow. In this article the Menter Shear Stress Transport (SST)  $k-\omega$  model coupled or not with a transition model from Menter et al. (2004) is used for comparison.

### 3. Reynolds Stress Models

Another type of RANS turbulence models are the differential Reynolds Stress Models where an equation is written and solved for each component of the symmetric Reynolds tensor defined as:

$$\bar{\rho}\tilde{R}_{ij} = \overline{\rho u_i'' u_j''} \quad (1)$$

where the superscript  $\bar{\cdot}$  denotes the simple average and  $\tilde{\cdot}$  the Favre (or mass) average and  $'$  (which appears later on) and  $''$  define the corresponding fluctuations.

RSM is also referred to as second-order closure model. This means that the second order correlations for the fluctuating velocity components are computed while the higher correlations are modeled.

In order to obtain the equations describing the Reynolds stresses the first momentum of the Navier-Stokes equation is considered. This is done by multiplying the equation by a fluctuating velocity component and time averaging the product. If  $\bar{N}$  is the operator that represents the Navier-

Stokes equation, then we obtain the Reynolds Stress equation from Wilcox (1993):

$$\overline{u_i'' N(\tilde{U}_j) + u_j'' N(\tilde{U}_i)} \quad . \quad (2)$$

After reorganizing the various terms, the final transport equations read as follows:

$$\frac{\partial}{\partial t}(\bar{\rho}\tilde{R}_{ij}) + \frac{\partial}{\partial x_k}(\bar{\rho}\tilde{U}_k\tilde{R}_{ij}) = \bar{\rho}P_{ij} + \bar{\rho}\Pi_{ij} - \bar{\rho}\epsilon_{ij} + \bar{\rho}D_{ij} + \bar{\rho}M_{ij} \quad . \quad (3)$$

The terms that appear at the right hand side of the equation represent the production, the redistribution, the destruction, the diffusion and the contribution of the turbulent mass flux, respectively.

The production term does not need modeling because it only depends on quantities for which an equation is solved,

$$\bar{\rho}P_{ij} = -\bar{\rho}\tilde{R}_{ik}\frac{\partial\tilde{U}_j}{\partial x_k} - \bar{\rho}\tilde{R}_{jk}\frac{\partial\tilde{U}_i}{\partial x_k} \quad . \quad (4)$$

The other terms, that is to say the re-distribution term

$$\bar{\rho}\Pi_{ij} = p' \left( \frac{\partial u_i''}{\partial x_j} + \frac{\partial u_j''}{\partial x_i} \right) \quad , \quad (5)$$

the destruction term

$$\bar{\rho}\epsilon_{ij} = \tau'_{ik}\frac{\partial u_j''}{\partial x_k} + \tau'_{jk}\frac{\partial u_i''}{\partial x_k} \quad , \quad (6)$$

the diffusion term

$$\bar{\rho}D_{ij} = -\frac{\partial}{\partial x_k} [\overline{\rho u_i'' u_j'' u_k''} + (\overline{p' u_i''} \delta_{jk} + \overline{p' u_j''} \delta_{ik}) - (\overline{\tau'_{ik} u_j''} + \overline{t'_{jk} u_i''})] \quad (7)$$

and the contribution of the turbulent mass flux due to the compressibility effects

$$\bar{\rho}M_{ij} = \overline{u_i''} \left( \frac{\partial \bar{\tau}_{jk}}{\partial x_k} - \frac{\partial \bar{p}}{\partial x_j} \right) + \overline{u_j''} \left( \frac{\partial \bar{\tau}_{ik}}{\partial x_k} - \frac{\partial \bar{p}}{\partial x_i} \right) \quad (8)$$

need to be modeled. The way the terms are modeled determines the particular type of Reynolds Stress Model.

#### 3.1. Reynolds Stress Transport Equation

The model chosen to be implemented in QUADFLOW is the SSG/LRR- $\omega$  turbulent model in which the Menter  $\omega$ -equation has been used to provide the length scale (Menter (1994)). This model has been developed by Eisfeld (Eisfeld (2004)) and is the combination of the LRR model near the wall (Launder et al. (1975)) and the SSG model (Speziale et al. (1991)) in the far field. The blending function of Menter has

been employed to blend the coefficients of the two models.

The re-distribution term is modeled as follows

$$\begin{aligned} \bar{\rho}\Pi_{ij} = & -(C_1\bar{\rho}\epsilon + \frac{1}{2}C_1^*\bar{\rho}P_{kk})\tilde{b}_{ij} \quad (9) \\ & + C_2\bar{\rho}\epsilon(\tilde{b}_{ik}\tilde{b}_{kj} - \frac{1}{3}\tilde{b}_{mn}\tilde{b}_{mn}\delta_{ij}) \\ & + (C_3 - C_3^*\sqrt{II})\bar{\rho}\tilde{k}\tilde{S}_{ij}^* \\ & + C_4\bar{\rho}\tilde{k}(\tilde{b}_{ik}\tilde{S}_{jk} + \tilde{b}_{jk}\tilde{S}_{ik} - \frac{2}{3}\tilde{b}_{mn}\tilde{S}_{mn}\delta_{ij}) \\ & + C_5\bar{\rho}\tilde{k}(\tilde{b}_{ik}\tilde{W}_{jk} + \tilde{b}_{jk}\tilde{W}_{ik}) \quad , \end{aligned}$$

where all the coefficients are obtained inserting the values in Table (1) in the blending function (23) described below. In the above equation  $\tilde{k}$  is the turbulent kinetic energy

$$\tilde{k} = \frac{\tilde{R}_{kk}}{2} \quad (10)$$

and  $\epsilon$  is the specific dissipation

$$\epsilon = C_\mu\tilde{k}\omega \quad , \quad (11)$$

where  $C_\mu$  is constant and equal to 0.09. The tensor appearing in equation (9) are the anisotropy tensor

$$\tilde{b}_{ij} = \frac{\tilde{R}_{ij}}{2\tilde{k}} - \frac{\delta_{ij}}{3} \quad , \quad (12)$$

and  $II$  its second invariant

$$II = \tilde{b}_{ij}\tilde{b}_{ij} \quad , \quad (13)$$

the strain rate tensor

$$\tilde{S}_{ij} = \frac{1}{2} \left( \frac{\partial\tilde{U}_i}{\partial x_j} + \frac{\partial\tilde{U}_j}{\partial x_i} \right) \quad , \quad (14)$$

the rotation tensor

$$\tilde{W}_{ij} = \frac{1}{2} \left( \frac{\partial\tilde{U}_i}{\partial x_j} - \frac{\partial\tilde{U}_j}{\partial x_i} \right) \quad (15)$$

and the traceless strain rate tensor  $\tilde{S}_{ij}^*$ .

Table 1. Coefficients of SSG and LRR model for the re-distribution term Eisfeld (2004)

	$C_1$	$C_1^*$	$C_2$	$C_3$	$C_3^*$	$C_4$	$C_5$
SSG	3.4	1.8	4.2	0.8	1.3	1.25	0.4
LRR	3.6	0	0	0.8	0	2.0	1.11

The isotropic destruction term for both models reads:

$$\bar{\rho}\epsilon_{ij} = \frac{2}{3}C_\mu\bar{\rho}\tilde{k}\omega\delta_{ij} \quad . \quad (16)$$

For what concerns the diffusion term the generalized gradient diffusion model is chosen:

$$\bar{\rho}D_{ij} = \frac{\partial}{\partial x_k} \left[ \left( \bar{\mu}\delta_{kl} + D^{(GGD)}\frac{\rho}{\omega}\tilde{R}_{kl} \right) \frac{\partial\tilde{R}_{ij}}{\partial x_l} \right] \quad (17)$$

The value of the constant  $D^{(GGD)}$  is computed by the equation:

$$D^{(GGD)} = F\sigma^* + (1-F)\frac{C_s}{C_\mu} \quad . \quad (18)$$

$F$  is the blending equation in (23),  $\sigma^* = 0.5$  and  $C_s = 0.22$ .

Finally the term  $\bar{\rho}M_{ij}$  is neglected.

The Menter  $\omega$ -equation for RSM reads as follows:

$$\frac{\partial}{\partial t}(\bar{\rho}\omega) + \frac{\partial}{\partial x_k}(\bar{\rho}\tilde{U}_k\omega) = \quad (19)$$

$$\bar{\rho}P^\omega - \bar{\rho}D^\omega + \frac{\partial}{\partial x_k} \left[ \left( \bar{\mu} + \sigma_\omega\frac{\bar{\rho}\tilde{k}}{\omega} \right) \frac{\partial\omega}{\partial x_k} \right] + \bar{\rho}C_D$$

with the production term

$$\bar{\rho}P^\omega = -\alpha_\omega\frac{\omega}{k}\tilde{R}_{ik}\frac{\partial\tilde{U}_i}{\partial x_k} \quad , \quad (20)$$

the destruction term

$$\bar{\rho}D^\omega = \beta_\omega\bar{\rho}\omega^2 \quad (21)$$

and the cross-diffusion term

$$\bar{\rho}C_D = \sigma_d\frac{\bar{\rho}}{\omega}\max\left(\frac{\partial\tilde{k}}{\partial x_k}\frac{\partial\omega}{\partial x_k}; 0\right) \quad . \quad (22)$$

The coefficients of the  $\omega$ -equation as well as those of the Reynolds stresses are blended using the following function:

$$\phi = F\phi^{LRR} + (1-F)\phi^{SSG} \quad (23)$$

The coefficient for the  $\omega$ -equation are listed in table (2).

Table 2. Coefficients for  $\omega$ -equation Eisfeld (2004)

	$\alpha_\omega$	$\beta_\omega$	$\sigma_\omega$	$\sigma_d$
SSG	0.44	0.0828	0.856	$2\sigma_\omega$
LRR	0.5556	0.75	0.5	0

The blending function of Menter is defined as:

$$F = \tanh(\zeta^4) \quad (24)$$

with

$$\zeta = \min \left[ \max \left( \frac{\sqrt{\tilde{k}}}{C_\mu \omega d}; \frac{500 \bar{\mu}}{\bar{\rho} \omega d^2} \right); \frac{4 \sigma_\omega^{(SSG)} \bar{\rho} \tilde{k}}{\bar{\rho} C_D^{(SSG)} d^2} \right]. \quad (25)$$

### 3.2. Boundary Conditions

At the inflow the following free stream conditions have been imposed:  $M=8.3$ ,  $Re=3.76 \times 10^6$  and  $T=102$ . For what concerns the turbulent variables a turbulent intensity of 0.5 is chosen. At the supersonic outflow the flow variables are extrapolated from inside the domain.

At the solid wall the non-slip condition is imposed for the velocity components and for the Reynolds stresses. For the  $\omega$ -equation, the Menter approach is chosen at the wall with constant wall temperature, in our case  $T_w=300K$ .

### 3.3. Computations

The QUADFLOW simulations have been performed on the linux-cluster of the Rechenzentrum at RWTH Aachen University. For each simulation 4 processors have been employed and the parallel computation is based on the MPI formulation. The QUADFLOW software has been validated during the years and a continuous validation is performed by the users and its developers.

For what concerns the newly implemented Reynolds Stress Model, simulations for subsonic flat plate have been performed with or without adaptation and the results compared with those obtained with different turbulence models like SST model or Spalart-Allmaras and with the analytical turbulent solution. The results of the validation on the hypersonic double ramp are discussed later on in this paper.

## 4. Implementation

The implementation of the RSM into the QUADFLOW solver can be divided into basically five steps. First of all some modifications have been required to add an additional turbulence model with a different number of equations with respect to those already available. The RSM is, in fact, a 7-equation turbulence model while the most common eddy viscosity models have one or two turbulence equations.

After that, the source terms have been implemented as well as their derivatives. These are employed both for the implicit time integration for the computation of the Jacobian matrix and for the explicit time integration, since the turbulent source terms are always treated implicitly.

As a third step, the viscous fluxes have been considered. On the one hand the viscous fluxes for the Reynolds stresses needed to be added to the solver. On the other hand the viscous fluxes of the momentum and energy equations needed to be modified by adding the contribution of the

Reynolds Stress to the mean flow. In contrast to eddy viscosity models, these additional terms are not represented by the turbulent viscosity but by the components of the Reynolds stresses themselves. Furthermore, the derivatives of the viscous fluxes are needed for implicit time integration.

The last part of the work consisted of implementing the boundary conditions at solid walls, the far field conditions, the initial conditions and the non-dimensional form of the Reynolds Stress.

Some further routines have been modified to limit the values of the variables, to add the constants that appear in the model and to compute the turbulent viscosity from the model variables. For what concerns the computation of the convective fluxes, no further implementation has been required.

## 5. Results

In this paper the validation on the hypersonic double wedge is presented (Bosco (2008)). The results obtained with the newly implemented Reynolds Stress Model are compared with experimental results obtained at the wind tunnel in Aachen (Neuenhahn (2006)) and numerical results obtained with the SST model coupled or not with a transition model (Krause (2008)). For what concerns the double ramp configuration, results obtained with adaptive grids are at the moment not yet available but these simulations are planned for the next future.

The hypersonic double wedge has been studied both with sharp and blunt leading edge and the computational grid for the configuration with nose, presented in Figure 2, is composed by 115000 cells. The sharp leading edge grid is obtained by the previous one removing the grid block for the nose.

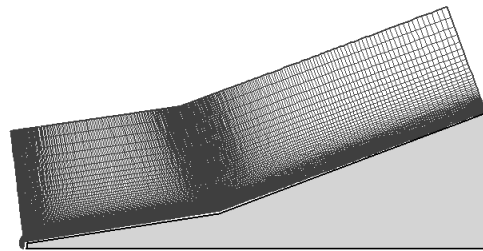


Figure 2. Computational grid

In order to obtain a realistic laminar behavior along the first ramp, a laminar condition is imposed there putting the turbulent source terms to zero. This allows to have a laminar/turbulent transition and to well capture the separation of the boundary layer along the first ramp. The results for fully turbulent simulations are also included in this study.

Figure 3 shows the behavior of the pressure coefficient along the wall for a configuration with nose. The grey horizontal lines represent the pres-

sure values obtained from the theory of oblique shock. We notice that the pressure value along the first ramp is the same for all the computational results but it is lower than the experimental one. This indicates us that probably the inflow conditions for the experimental test were different from the nominal ones later used for the simulations. A higher pressure value is also observed along the second ramp where the pressure peak achieved in the wind tunnel is not reached by the simulations. The fully turbulent profile obtained with the RSM is in good agreement with the SST model except toward the end of the second ramp where a higher pressure coefficient can be observed. The cause of this behavior is still under investigation.

For what concerns the laminar/turbulent computation, it can be noticed that the boundary layer separates along the first ramp but the size of the separation is smaller than that shown by the laminar solution. After the kink the pressure increases, as predicted by the theory, with a slope bigger than in the laminar case and reaches the theoretical value. Along the second ramp a further change in the pressure coefficient can be observed due to the merging of the two shock waves.

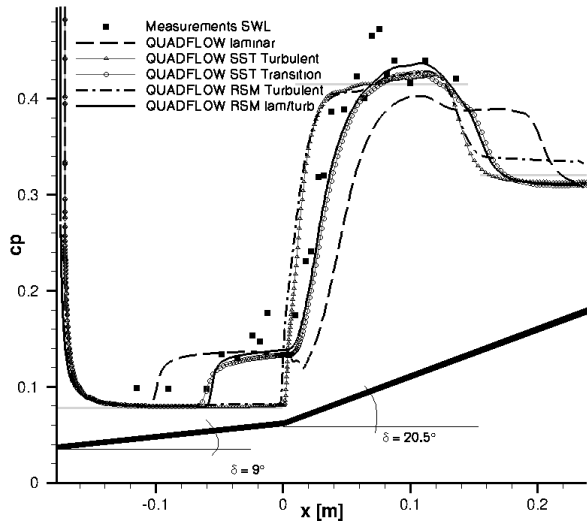


Figure 3. Pressure coefficient distribution along a double wedge configuration with blunt leading edge.

The Stanton coefficient is shown in Figure 4. A laminar/turbulent simulation, with the Reynolds Stress Model, has been performed here while the fully turbulent solution does not capture the separation of the boundary layer and shows values significantly different from the experimental results. For what concerns the RSM with laminar first ramp, the Stanton number decreases correctly along the first ramp following the laminar result and a further abrupt decrease occurs when the separation takes place. Also in this case, the size of the separation is smaller than that observed in a laminar simulation. After the kink the Stanton number recovers but the values it takes are always higher than those from the wind tunnel experiment. With respect to the SST Menter model, the RSM shows a smaller Stanton peak along the second ramp but no experimental results are avail-

able for comparison along the second part of the second ramp.

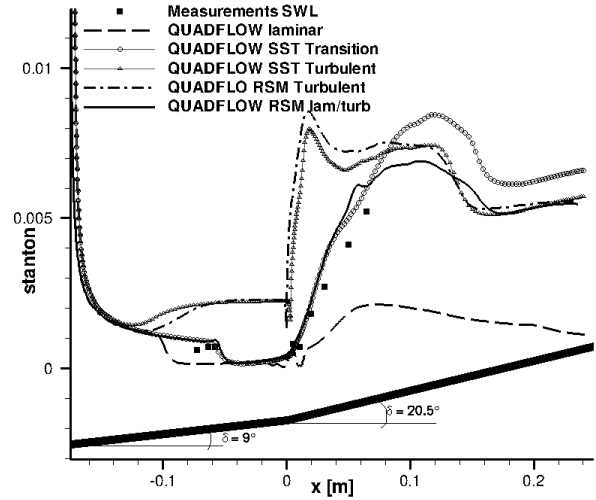


Figure 4. Stanton number distribution along a double wedge configuration with blunt leading edge.

In Figure 5 the pressure coefficient profile for a sharp leading edge is shown. The grey horizontal lines represent the values obtained from the oblique shock theory. The experimental results along the first ramp match the computational value. In the sharp leading edge test case we do not notice a big difference between the laminar result and the result obtained with the laminar/turbulent RSM or the SST Menter model with transition. In both computational cases the value of the pressure along the separation and up to the peak value are well predicted. For what concerns the results toward the end of the second ramp a good agreement with computational results is observed.

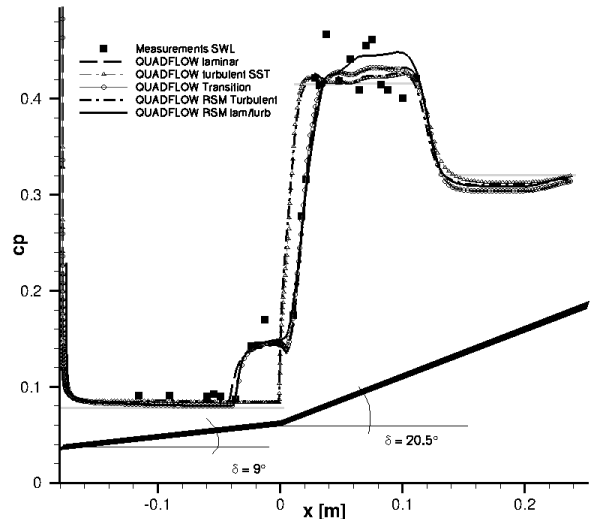


Figure 5. Pressure coefficient distribution along a double wedge configuration with sharp leading edge.

Figure 6 shows the Stanton coefficient for a sharp leading edge double wedge configuration.

As in the case with blunt leading edge, the full turbulent simulation largely over-predicts the value of the Stanton number along the first ramp. On the other side the laminar/turbulent RSM result and the SST transition result perfectly match the laminar profile and the differences in the separation region are small. After decreasing because of the separation, the Stanton number recovers after the kink where the second shock wave occurs and the numerical values well fit the experimental ones. The peak value on the second ramp is however not reached by the numerical simulations. The computational profiles toward the end of the second ramp are in good agreement.

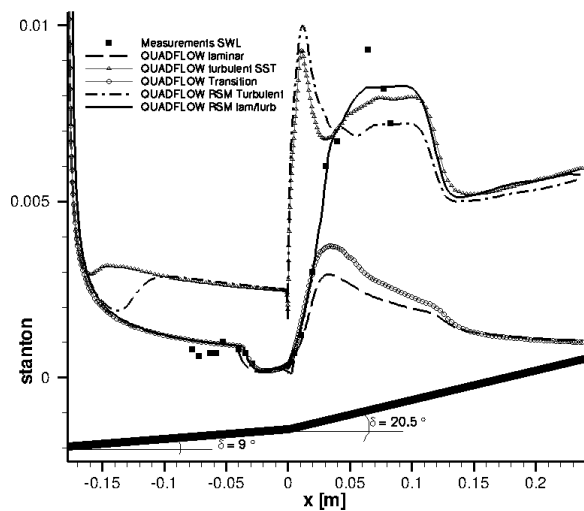


Figure 6. Stanton number distribution along a double wedge configuration with sharp leading edge.

## 6. Outlook

The implementation of the RSM in QUADFLOW solver has now been completed and the model has been validated on different test cases. At the moment, some grid convergence studies are being performed in order to find the grid that produces the best result, combined with the Reynolds stress model, at the lower computational effort. Further on a complete three dimensional hypersonic inlet will be studied and the influence of the side wall as well as three dimensional phenomena will be analyzed. Because of their anisotropic characteristics the RSMs are expected to produce considerably better results in three dimensional simulations with respect to eddy viscosity models. In the near future simulations with adaptive grids both for three dimensional and two dimensional double wedge are planned.

## 7. Acknowledgments

Financial support from the Deutsche Forschungsgemeinschaft (German Research Association) through grant GSC 111 and Research Training Group GRK 1095/1 is gratefully acknowledged.

## References

- Eisfeld B (2004) Implementation of Reynolds stress models into the DLR-FLOWER code. Internal DLR report IB 124-2004/31
- Eisfeld B, Brodersen O (2005) Advanced Turbulence Modelling and Stress Analysis for the DLR-F5 Configuration. AIAA Applied Aerodynamics Conference
- Bramkamp F, Lamby Ph, Müller S (2004) An adaptive multiscale finite volume solver for unsteady and steady state flow computations. *J. of Computational Physics* 197:460-490
- Kroll N, Rossow CC, Becker K, Thiele F (2000) The MEGAFLOW Project. *J. of Aerospace Science and Technology* 4:223-237
- Batten P, Leschziner MA, Goldberg UC (1997) Average-State Jacobians and Implicit Methods for Compressible Viscous and Turbulent Flows. *J. of Computational Physics*, 137 :38-78
- Reinartz B, Ballmann J (2007) Computation of Hypersonic Double Wedge Shock/Boundary Layer Interaction. 26th International Symposium on Shock Waves
- Menter F, Langtry R (2004) A Correlation-Based Transition Model Using Local Variables Part 1- Model Formulation. Proceeding of ASME Turbo Expo
- Wilcox DC (1993) Turbulence Modelling for CFD. DCW Industries Inc
- Menter FR (1994) Two-Equation Eddy-Viscosity Turbulence Models for Engineering Applications. *AIAA J.* 32:1598-1605
- Lauder BR, Reece GJ, Rodi W (1975) Progress in the development of a Reynolds-stress turbulence closure. *J. of Fluid Mechanics* 68:537-566
- Speziale CG, Sarkar S, Gatski TB (1991) Modelling the pressure-strain correlation of turbulence: an invariant dynamical system approach. *J of Fluid Mechanics* 227:254-272
- Batten P, Leschziner MA, Goldberg UC (1997) Average-State Jacobians and Implicit Methods for Compressible Viscous and Turbulent Flows. *J. of Computational Physics*, 137:38-78
- Bosco A, Reinartz BU, Müller S (2008) Reynolds Stress Model implementation for hypersonic flow simulations. DGLR Kongress 2008 Darmstadt 23-25 Sept 2008
- Neuenhahn T, Olivier H (2006) Influence of the wall temperature and the entropy layer effects on double wedge shock boundary layer interactions. AIAA Paper 2006-8136
- Krause M, Ballmann J (2008) Application of a correlation-based intermittency transition model for hypersonic flows. DGLR Kongress 2008 Darmstadt 23-25 Sept 2008